Research Article

The synthesis, characterization and application of the binol-cages of R-/S-enantiomers

Tianyu Li, Luyao Ding, Yihong Kang, Xin-Qi Hao, Yujing Guo*, **Linlin Shi***, **Mao-Ping Song**

College of Chemistry, Zhengzhou University, Zhengzhou 450001, Henan, China.

*Correspondence to:** Prof. Linlin Shi, College of Chemistry, Zhengzhou University, No.100 Science Avenue, Zhengzhou 450001, Henan, China. E-mail: linlinshi@zzu.edu.cn; Prof. Yujing Guo, College of Chemistry, Zhengzhou University, No.100 Science Avenue, Zhengzhou 450001, Henan, China. E-mail: yujingguo@zzu.edu.cn

Abstract

In the past few years, significant efforts have been made to create and self-assemble covalent organic cages with increased complexity and functionality. However, although supramolecule cages have been widely recognized as probes to identify metal ions, the detection of mercury ions has not been fully developed. Here, we have designed and synthesized a pair of chiral cages with custom cavities based on the unique rigid structure of 1, 10-binaphthol (binol). Meanwhile, the supramolecular cage has excellent performance in high sensitivity and selectivity for detecting mercury ions. The UV titration results indicate that the binding ratio of the host to guest is 1:5. The titration curve conforms to the nonlinear fitting of the Hill function, which can obtain the binding constant K = 2.57×10^5 M^{-1}. Furthermore, the detection limit of 1.9×10^{-7} M can be obtained because the absorbance of cages exhibits a strong linear relationship with Hg^{2+} concentrations. This work provides a new method for selective recognition of ions by supramolecular cages.

Keywords: Covalent organic cage, mercury ion, detection, chemiluminescence, self-assembly

INTRODUCTION

The global attention on environmental pollution caused by heavy metal ions persists due to their potential to inflict severe harm on both animals and humans[1]. Many highly sensitive and selective probes have been developed and successfully used in practical life in order to detect metal ions in the environment. For

example, probes synthesized by Mohandoss *et al.* were widely used for detecting Fe^{3+}, Al^{3+}, Cu^{2+}, and Ag^+ ions[2-4]. As is well known, mercury is extremely harmful to organisms and the environment, especially to mammals. It can not only enter the human body directly through the skin, digestive system, or respiratory system but also accumulate in the environment, ultimately entering the human body through the food chain and causing serious damage to the central nervous and endocrine systems of the human body. In addition, all stable forms of Hg (i.e., metallic, inorganic, and organic) cause neurological poisoning in fish, wildlife, and humans. It causes several disorders in the liver, kidney, heart, stomach, brain, intestine, and immune system[5-7]. According to the United States Environmental Protection Agency (US EPA), the maximum possible limit of Hg^{2+} ions in drinking water is 2 ppb, but the amount of Hg^{2+} ions in drinking water excess to the limit may pose a risk to human health and the environment (Environmental Protection Agency, 2001). Despite these drawbacks, mercury and mercury salts still widely exist in nature in the form of elemental mercury, inorganic, and organic compounds. Human activities, industrial production, and natural phenomena can all lead to the production of various forms of mercury compounds[8-10]. Therefore, it is necessary to seek efficient, simple, and fast new ways to detect mercury ions in the atmosphere and wastewater in order to protect the Earth's environment[11-25].

In recent years, mercury ions have been detected by a large number of analytical methods, including cold vapor atomic fluorescence spectroscopy[26], inductively coupled plasma mass spectrometry (ICP-MS)[27], gas chromatography[28], neutron activation analysis (NAA)[29], and high-performance liquid chromatography[30]. However, these technologies often require cumbersome operations and expensive instruments. As a result, the development of more efficient and facile approaches for mercury ion detection is highly appealing yet challenging.

Supramolecular chemistry, as an interesting field, has successively attracted much attention due to its unique structures and extensive applications in sensing[31,32], catalysis[33,34], separation[35,36], gas adsorption[37,38], biological imitation[39], and so on[40,41]. The intriguing three-dimensional molecular cages have proven to be superior alternative architectures, garnering considerable interest owing to their outstanding structures, properties, applications, and the diverse array of charming skeletons successfully generated via coordinative self-assembly, such as octahedrons[42,43], tetrahedrons[44-47], spirals[48], capsules[49], *etc*. Additionally, subcomponent self-assembly, as the most powerful bottom-up strategy, has attracted great attention by preparing highly organized structures with different functions in an "order-out-of-chaos" and well-controlled manner[50-53]. Comparatively, the discrete supramolecular structures formed by covalent bonds remain underdeveloped, possibly due to the dynamic and unstable interactions[54,55]. In this context, molecular cages formed by imine condensation have developed rapidly[56-58] since the groundbreaking work of Quan *et al.* in 1991[59]. Despite the impressive progress made by chemists in this field, the involvement of multiple functional components in a single supramolecular system causes further difficulties for synthesis and its evocative biological heuristic process. Meanwhile, there are relatively few examples of detecting mercury ions as fluorescent probes, although covalent supramolecular cages have been widely reported as examples of fluorescent probes[60-64]. Therefore, it is crucial to create novel covalent supramolecular cages and use them for mercury ion detection.

Herein, we purposefully designed and constructed covalent organic cages with (*R*)- or (*S*)-binaphthyl skeletons as ligands and tri(2-aminoethyl)amine as vertices by amine aldehyde condensation-driven collaborative self-assembly. Notably, the ether chains were introduced on three symmetric binaphthyl ligands to form 20-crown-6. In addition, mercury ions were successfully recognized through fluorescence testing. To our delight, these covalent organic nanocages, which possess chemiluminescent properties, can serve as a fluorescence sensor to detect these ions. The successful synthesis of the cage had been

demonstrated by NMR, mass spectrometry, Fourier transform infrared (FT-IR), and molecular simulations.

RESULTS AND DISCUSSION

As shown in Scheme 1, our investigation was commenced by using the compound **1** [3, 6, 9, 12-tetraoxatetradecane-1, 14-diol] and compound **3** (*R*)- or (*S*)-BINOL (binaphthol) as the starting substrates. Initially, (*S*)-**4** was treated with potassium *t*-butoxide at 75 °C, and the resultant system was reacted with pentaethylene glycol di-*p*-toluenesulfonate **2** to afford the product (*S*)-**5** in 40% yield. A Suzuki coupling reaction of bromide (*S*)-**5** with 4-formylphenylboronic acid gave an important precursor (*S*)-**7** in 30% yield, which has two aldehyde functionalities attached to the binaphthyl backbone. On the basis of the successful synthesis of (*S*)-**7**, covalent organic nanocage cage (*S*)-**8** was prepared by co-self-assembly with tris(2-aminoethyl)amine in a yield of 55% as a yellow solid. The same method was used to synthesize (*R*)-**8** for a 53% yield. The chemical structures of these chiral cages were adequately characterized by ^{1}H NMR, mass spectrometry, and correlation spectroscopy (COSY) spectral information.

The desired covalent organic cages were successfully synthesized according to ^{1}H NMR spectroscopy [Supplementary Figures 1-20]. As shown in Figure 1, the protons H^a-H^g located on the binaphthyl backbone and phenyl moiety were represented by eight independent sets of peaks in the spectra of both ligand **7** and cage **8**. It is worth noting that the characteristic peak of aldehyde in the **7** disappeared due to the condensation with amine, indicating that compound **7** was completely reacted. Moreover, the signal of Schiff base hydrogen appeared at 8.01 ppm, also proving the successful synthesis of the target cage structure. Chemical shifts were observed for protons H^a (from 7.96 ppm to 7.43 ppm) and H^b (from 7.84 ppm to 6.99 ppm), as compared with the free aromatic ligand **7**, because of the electronic effect on the imine group. 2D NMR spectroscopies, such as COSY and diffusion-ordered spectroscopy (DOSY), provided more precise structural data in support of the formation of covalent organic cages [Supplementary Figures 21 and 22]. Moreover, additional evidence for the formation of [2+3] imine cages could also be provided by electrospray ionization mass spectrometry (ESI-MS). Experimental isotope patterns for the peak of [**8**+2H]$^{2+}$ are strongly consistent with theoretical isotope patterns, suggesting that covalent organic supramolecular cages were constructed successfully via self-assembly. All main peaks of mass spectra also indicated the formation of corresponding cage architectures [Figure 1E and Supplementary Figure 23].

FT-IR characterization has also proven to be an important tool for detection of changes in functional groups [Figure 2]. The infrared spectrum of compound (*S*)-**7** displayed a strong aldehyde stretching vibrational peak at 1,695 nm alongside a stretching vibration peak at 1,642 nm due to the imine formation.

The UV-Vis and fluorescence spectra also show the structural characteristics of the cage, as shown in Figure 3; the UV-Vis absorption spectra for the cage display two main peaks at 322 nm and 280 nm, which correspond to the *n*-π^* transitions (C=N) and π-π^* transitions (C=C). The UV-Vis absorption spectra for the ligand exhibited a unique peak at 337 nm, which was attributed to the existence of *n*-π^* transitions (C=O). Furthermore, the emission wavelengths of (*S*)-**8** and (*S*)-**7** are 414 nm and 458 nm in the fluorescence spectra, respectively.

A simulated molecular model of cages was constructed due to many unsuccessful efforts to obtain the crystal structure of cages [Figure 4 and Supplementary Figure 24]. Analysis of the simulated cages showed the expected [2+3] structure, with two amine moieties connected by three side arms based on binol in the top and bottom views. The structure of cages had a C_3 symmetric topology and three C_2 axes perpendicular to the C_3 axis.
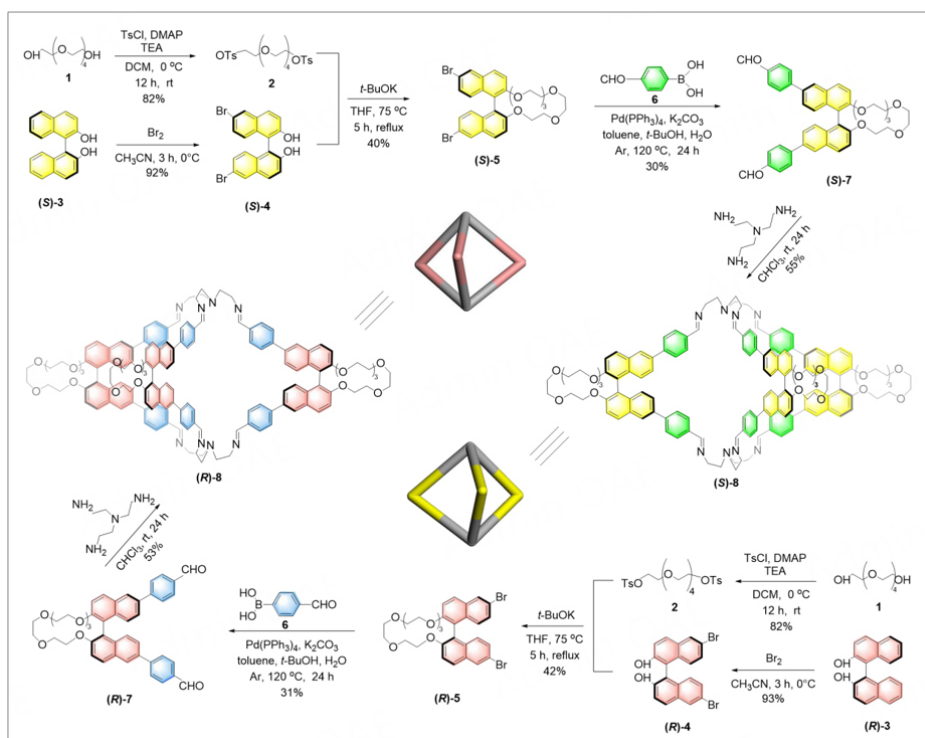
Scheme 1. Synthetic route to chiral organic cages.
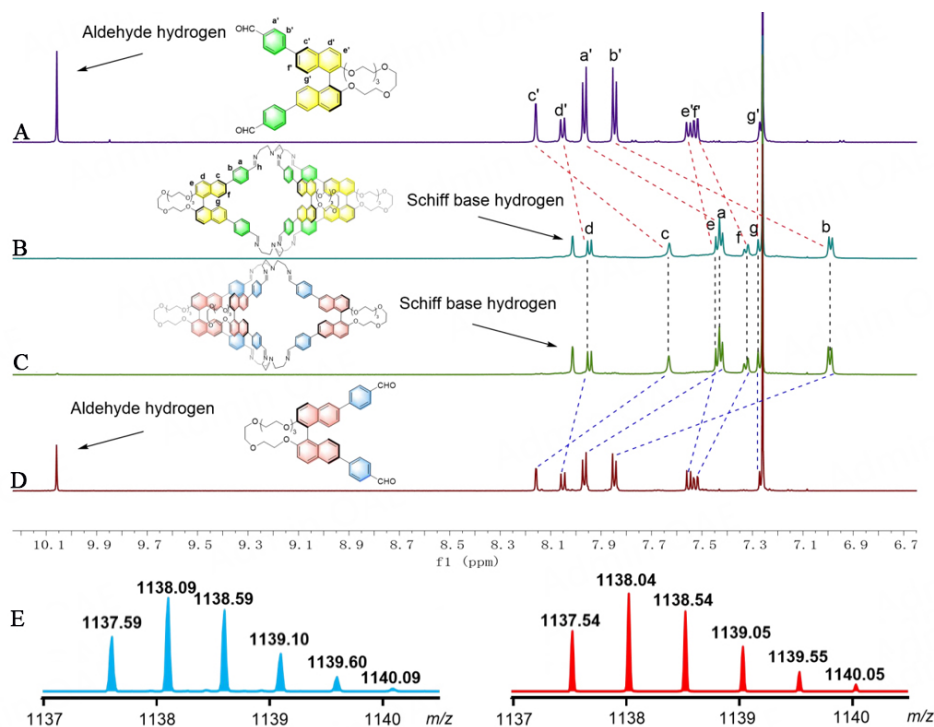
Figure 1. Part of the ^{1}H NMR (600 MHz, CDCl$_3$, 22 $^\circ$C) spectra of **(S)-7** (A); **(S)-8** (B); **(R)-8** (C); **(R)-7** (D) and experimental ESI-MS of the **(S)-8** of [8+2H]$^{2+}$ (blue) and simulated mass spectra (red) (E).
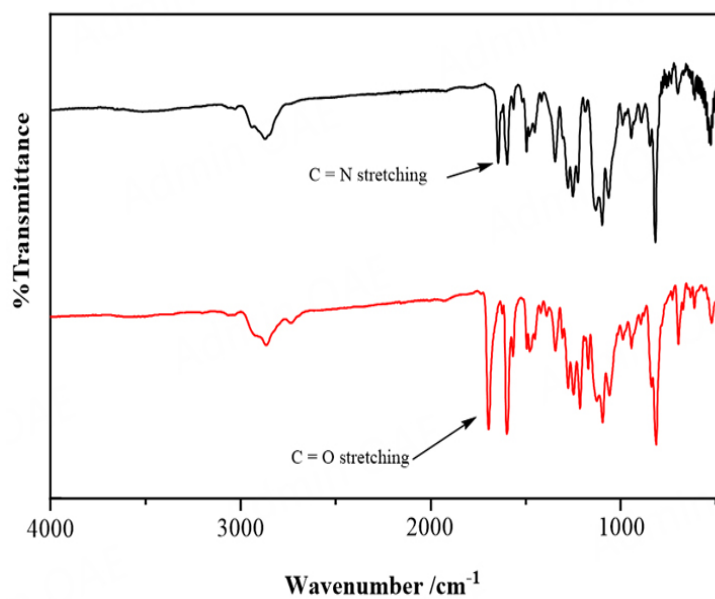
Figure 2. Fourier transform infrared spectroscopy of **cage** (black line) and compound **7** (red line).

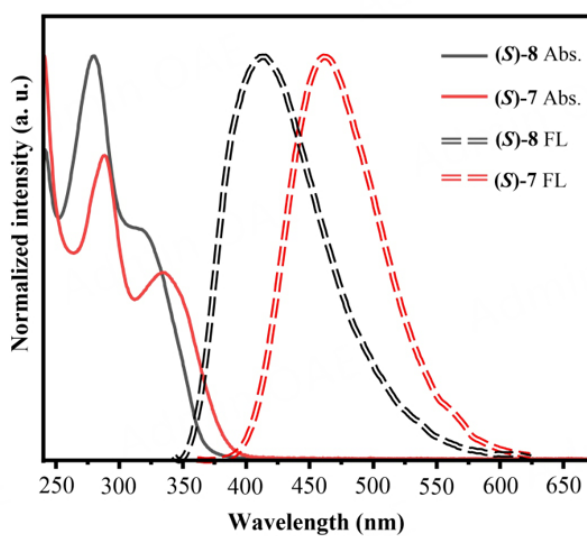**Figure 3.** UV-Vis and fluorescence spectra of compound **(S)-7** and **(S)-8**.

The inherent chirality of imine cages was characterized by circular dichroism (CD) spectroscopy. As shown in Figure 5, (*R*)-**8** and (*S*)-**8** exhibited mirror CD spectra with highly pronounced Cotton effects in the wavelength range of 240 to 400 nm. The CD spectra of cages displayed one strong band at 286 nm, which
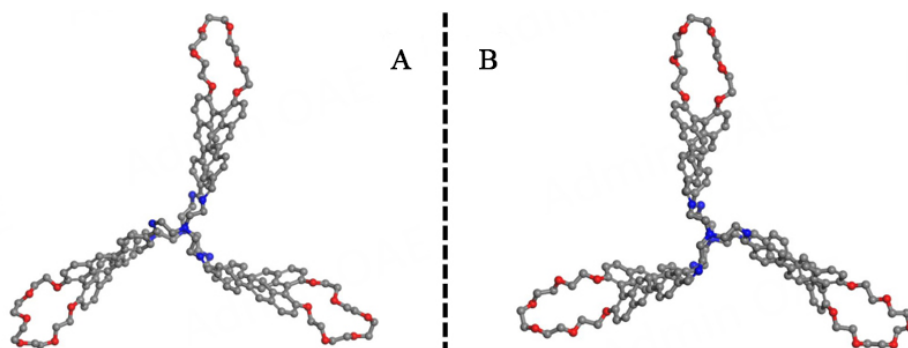
Figure 4. The simulated crystal structures of **(S)-8** (A) and **(R)-8** (B). (N, blue, O, red, C, gray, and hydrogens are omitted for clarity).
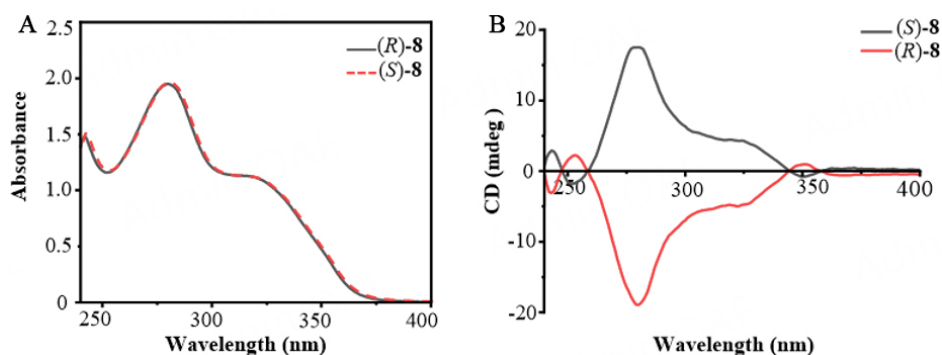

Figure 5. (A) The UV-Vis spectra of **(R)-8** and **(S)-8** in CDCl$_3$ (c = 0.01 mM); (B) CD spectra of (R)-8 and (S)-8 in CDCl3 (c = 0.1 mM).

indicated the absorption of naphthalene groups on the binaphthyl backbone. Therefore, we have successfully synthesized the covalent supramolecular cages through NMR, ESI-MS, molecular simulations, CD, and FT-IR characterization methods.

The heavy metal ion Hg^{2+} poses a significant threat to the environment due to its high affinity for thiol groups in proteins and enzymes. Additionally, it is important to note that mercury ions are not biodegradable. As a result, even at extremely low concentrations, they can have detrimental effects on the kidneys and brain, potentially leading to various diseases. The US EPA stipulates that the maximum concentration of mercury ions in drinking water is 10 μM. Consequently, in this work, the cage can be used as a fluorescence probe because adding mercury ions to the solution does not decompose the cage [Supplementary Figure 25]. As shown in the results, the fluorescence intensity of the supramolecule cage gradually increases with the increasing concentration of mercury ions [Figure 6A and B]. Meanwhile, the covalent supramolecule cage shows a redshift of 48 nm in the emission spectra. The addition of mercury ions created an umbrella-shaped structure that made the molecule more rigid. As a result, electron delocalization between the crown ether and imine parts became more viable. This enhanced dipole moment and charge separation, leading to a significant redshift of 48 nm in the fluorescence emission spectrum [Figure 6C][65,66]. Moreover, the UV-Vis titration experiment provided important quantitative information [Supplementary Figures 26-30]. As shown in Supplementary Figure 26, the absorbance at 280 nm gradually decreased and underwent a shift to red with the addition of mercury ions. The change remained basically unchanged after adding 5 eq. of mercury ions. Therefore, the binding ratio of 1:5 could be obtained by using the molar ratio plot [Supplementary Figure 28]. Two linearly fitted lines intersected at a point with a horizontal coordinate of 5 eq., proving that the binding ratio of the cage to mercury ions was 1:5.
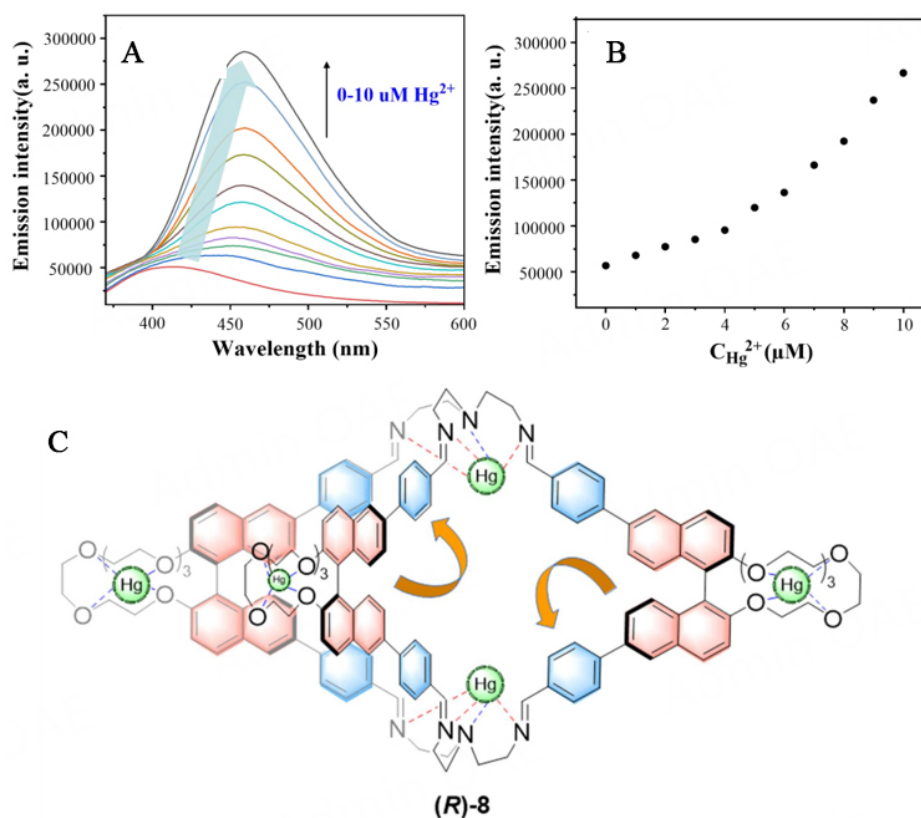
Figure 6. Fluorescence titration of **(R)-8** (10 μM) upon addition of Hg^{2+} ion up to 10 μM in CHCl$_3$ (A) and the plot of fluorescence intensity versus Hg^{2+} concentration (B) (λ_{ex} = 322 nm, Silt = 2, 2); (C) Mercury ion detection mechanism.

Meanwhile, the UV-Vis titration data could be well fitted by the Hill function. Based on the fitting results, the binding constant K = 2.57 × 10^5 M^{-1} could be obtained [Supplementary Figure 29]. Finally, the detection limit was calculated by showing a good linear relationship between the absorbance of the cage and 0-5 eq. of mercury ions at 280 nm [Supplementary Figure 30]. It was worth noting that the CD spectrum of the cage could also detect these ions. The CD spectrum underwent significant changes with the continuous addition of mercury ions. On the contrary, no significant changes were observed after the addition of copper ions, suggesting that copper ions could not bind to the cage [Supplementary Figure 27]. In order to prove that the cage can effectively recognize mercury ions, common metal ions are also used for detection [Figure 7]. It is obvious from Figure 7 that Hg^{2+} ions have the most fluorescence enhancement effect on the supramolecule cage.

In order to further explore the sensing ability of the cage for the Hg^{2+} ion, selective recognition experiments of the cage (0.2 mM) were also conducted by using different concentrations of Hg^{2+} (0.7, 1.4, 2.1 mM) in CHCl$_3$ [Figure 8]. The results, as depicted in Figure 8, exhibit distinct changes in color that can be obviously observed by the naked eye. The color of the CHCl$_3$ with spiked Hg^{2+} transformed from colorless to light yellow. The ability of cages to detect mercury ions in different pH solutions was also tested separately, and similar results were observed [Supplementary Figure 31]. In addition, the cage had been compared with supramolecular materials that were used for detecting mercury ions in recent years [Supplementary Table 1]. According to [Supplementary Table 1], the diverse detection methods of the cage possessed unique advantages. Therefore, it is possible to detect the presence of mercury ions without the use of any additional instruments and make the process more efficient and expedient.
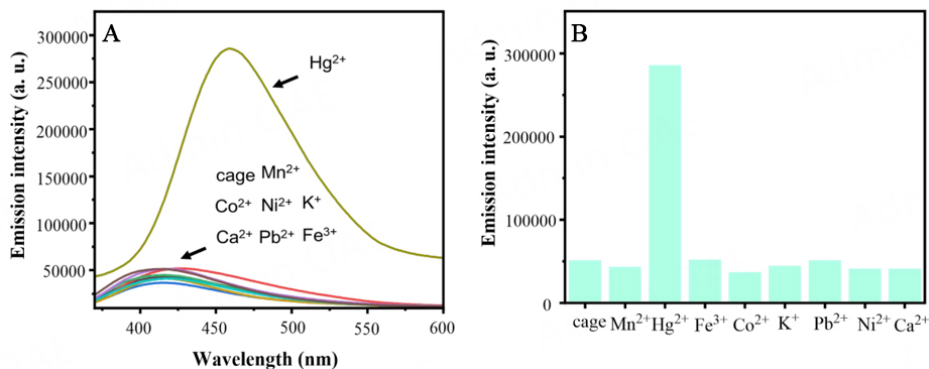
Figure 7. (A) Emission spectra and (B) bar graph of (*R*)-8 (10 μM) with various metal ions (10 μM) in CHCl$_3$ (λ_{ex} = 322 nm, slit width = 2, 2 nm).

Figure 8. Hg^{2+}ion detection diagram based on **(R)-8**.

CONCLUSIONS

In conclusion, we have demonstrated the formation of two chiral organic cages using chiral binaphthyl as the main building block. The structures of the chiral cages were characterized using ^{1}H NMR, 2D NMR, mass spectroscopy, molecular simulation, CD, and FT-IR characterization analyses. Furthermore, the absorbance of cages exhibited a good linear correlation with Hg^{2+} concentrations with detection limits of 1.9×10^{-7} M. On the other hand, the cage could be used for selective recognition of Hg^{2+} ions as a supramolecular probe, especially allowing for the direct observation of changes in solution systems, thereby contributing to the protection of environmental pollution, which may contribute to the development of new approaches for utilizing supramolecular cages as probes in the future.

DECLARATIONS

Acknowledgments
We acknowledge the Molecular Scale Lab for mass spectrometry characterization.

Authors' contributions
Designing the experiments, writing the manuscript, and being responsible for the whole work: Shi L, Guo Y, Song MP
Revising the first draft of the manuscript: Hao XQ
Performing the experiments and synthesizing the substrates: Li T, Ding L, Kang Y

Availability of data and materials
Please refer to the Supplementary Materials for the experimental procedures and characterization of the new compound.

Conflicts of interest
All authors declared that there are no conflicts of interest.

Ethical approval and consent to participate
Not applicable.

Consent for publication
Not applicable.

REFERENCES

1. Schwarzenbach RP, Escher BI, Fenner K, et al. The challenge of micropollutants in aquatic systems. *Science* 2006;313:1072-7. DOI
2. Mohandoss S, Ganesan S, Palanisamy S, et al. Nitrogen, sulfur, and phosphorus Co-doped carbon dots-based ratiometric chemosensor for highly selective sequential detection of Al^{3+} and Fe^{3+} ions in logic gate, cell imaging, and real sample analysis. *Chemosphere* 2023;313:137444. DOI
3. Mohandoss S, Palanisamy S, You S, Shim JJ, Lee YR. Rapid detection of silver ions based on luminescent carbon nanodots for multicolor patterning, smartphone sensors, and bioimaging applications. *Anal Methods* 2021;13:5719-26. DOI PubMed
4. Sonaimuthu M, Ganesan S, Anand S, et al. Multiple heteroatom dopant carbon dots as a novel photoluminescent probe for the sensitive detection of Cu^{2+} and Fe^{3+} ions in living cells and environmental sample analysis. *Environ Res* 2023;219:115106. DOI
5. Li X, Bian C, Meng X, Xiao F. Design and synthesis of an efficient nanoporous adsorbent for Hg^{2+} and Pb^{2+} ions in water. *J Mater Chem A* 2016;4:5999-6005. DOI
6. Mao X, Wang L, Wang C, Lichtfouse E. Glutathione-functionalized melamine sponge, a mimic of a natural antidote, as a quick responsive adsorbent for efficient removal of Hg(II) from aqueous solutions. *Environ Chem Lett* 2018;16:1429-34. DOI
7. Tajeu GS, Booth JN 3rd, Colantonio LD, et al. Incident cardiovascular disease among adults with blood pressure <140/90 mm Hg. *Circulation* 2017;136:798-812. DOI PubMed PMC
8. Wu P, Dou J, Xu Y, et al. Impact of engineering renovation on dynamic health risk assessment of mercury in a thermometer enterprise. *Front Public Health* 2022;10:1037915. DOI PubMed PMC
9. Recknagel S, Radant H, Kohlmeyer R. Survey of mercury, cadmium and lead content of household batteries. *Waste Manag* 2014;34:156-61. DOI PubMed
10. Mielke HW, Gonzales C. Mercury (Hg) and lead (Pb) in interior and exterior New Orleans house paint films. *Chemosphere* 2008;72:882-5. DOI PubMed

11. Ariya PA, Amyot M, Dastoor A, et al. Mercury physicochemical and biogeochemical transformation in the atmosphere and at atmospheric interfaces: a review and future directions. *Chem Rev* 2015;115:3760-802. DOI

12. Awual MR, Hasan MM, Eldesoky GE, Khaleque MA, Rahman MM, Naushad M. Facile mercury detection and removal from aqueous media involving ligand impregnated conjugate nanomaterials. *Chem Eng J* 2016;290:243-51. DOI

13. Chen GH, Chen WY, Yen YC, Wang CW, Chang HT, Chen CF. Detection of mercury(II) ions using colorimetric gold nanoparticles on paper-based analytical devices. *Anal Chem* 2014;86:6843-9. DOI PubMed

14. Chen G, Guo Z, Zeng G, Tang L. Fluorescent and colorimetric sensors for environmental mercury detection. *Analyst* 2015;140:5400-43. DOI

15. Ding Q, Li C, Wang H, Xu C, Kuang H. Electrochemical detection of heavy metal ions in water. *Chem Commun* 2021;57:7215-31. DOI

16. Guo Y, Wang Z, Shao H, Jiang X. Hydrothermal synthesis of highly fluorescent carbon nanoparticles from sodium citrate and their use for the detection of mercury ions. *Carbon* 2013;52:583-9. DOI

17. Gupta VK, Sethi B, Sharma R, Agarwal S, Bharti A. Mercury selective potentiometric sensor based on low rim functionalized thiacalix [4]-arene as a cationic receptor. *J Mol Liq* 2013;177:114-8. DOI

18. Lin ZH, Zhu G, Zhou YS, et al. A self-powered triboelectric nanosensor for mercury ion detection. *Angew Chem Int Ed Engl* 2013;52:5065-9. DOI

19. Shi Y, Li W, Feng X, et al. Sensing of mercury ions in porphyra by Copper @ gold nanoclusters based ratiometric fluorescent aptasensor. *Food Chem* 2021;344:128694. DOI

20. Wang L, Peng X, Fu H, Huang C, Li Y, Liu Z. Recent advances in the development of electrochemical aptasensors for detection of heavy metals in food. *Biosens Bioelectron* 2020;147:111777. DOI

21. Wang Y, Zhang L, Han X, Zhang L, Wang X, Chen L. Fluorescent probe for mercury ion imaging analysis: strategies and applications. *Chem Eng J* 2021;406:127166. DOI

22. Du J, Jiang L, Shao Q, et al. Colorimetric detection of mercury ions based on plasmonic nanoparticles. *Small* 2013;9:1467-81. DOI

23. Ali S, Chen X, Ahmad S, et al. Morphology-controllable bimetallic gold nanostructures for mercury detection: recent developments, challenges and prospects. *Arab J Chem* 2023;16:104997. DOI

24. Bansod B, Kumar T, Thakur R, Rana S, Singh I. A review on various electrochemical techniques for heavy metal ions detection with different sensing platforms. *Biosens Bioelectron* 2017;94:443-55. DOI

25. Hasan A, Nanakali NMQ, Salihi A, et al. Nanozyme-based sensing platforms for detection of toxic mercury ions: an alternative approach to conventional methods. *Talanta* 2020;215:120939. DOI

26. Pierce CE, Furman OS, Nicholas SL, et al. Role of ester sulfate and organic disulfide in mercury methylation in peatland soils. *Environ Sci Technol* 2022;56:1433-44. DOI

27. Miao J, Feng S, Dou S, et al. Association between mercury exposure and lung function in young adults: A prospective cohort study in Shandong, China. *Sci Total Environ* 2023;878:162759. DOI

28. Yang Y, Tan Q, Lin Y, et al. Point discharge optical emission spectrometer as a gas chromatography (GC) detector for speciation analysis of mercury in human hair. *Anal Chem* 2018;90:11996-2003. DOI

29. Kosta L, Byrne AR, Dermelj M. Trace elements in some human milk samples by radiochemical neutron activation analysis. *Sci Total Environ* 1983;29:261-8. DOI PubMed

30. Song Y, Guo F, Zeng P, Liu J, Wang Y, Cheng H. Simultaneous measurements of Cr, Cd, Hg and Pb species in ng L^{-1} levels by interfacing high performance liquid chromatography and inductively coupled plasma mass spectrometry. *Anal Chim Acta* 2022;1212:339935. DOI

31. Li W, Sun L, Liu C, et al. Supramolecular Fe^{II}4L$_4$ cage for fast ammonia sensing. *J Mater Chem C* 2022;10:9216-21. DOI

32. Zhang Z, Zhao Z, Wu L, et al. Emissive platinum(II) cages with reverse fluorescence resonance energy transfer for multiple sensing. *J Am Chem Soc* 2020;142:2592-600. DOI

33. Bhandari P, Mukherjee PS. Covalent organic cages in catalysis. *ACS Catal* 2023;13:6126-43. DOI

34. Ham R, Nielsen CJ, Pullen S, Reek JNH. Supramolecular coordination cages for artificial photosynthesis and synthetic photocatalysis. *Chem Rev* 2023;123:5225-61. DOI PubMed PMC

35. Bell DJ, Natrajan LS, Riddell IA. Design of lanthanide based metal-organic polyhedral cages for application in catalysis, sensing, separation and magnetism. *Coordin Chem Rev* 2022;472:214786. DOI

36. Hou YJ, Wu K, Wei ZW, et al. Design and enantioresolution of homochiral Fe(II)-Pd(II) coordination cages from stereolabile metalloligands: stereochemical stability and enantioselective separation. *J Am Chem Soc* 2018;140:18183-91. DOI

37. Giri N, Del Pópolo MG, Melaugh G, et al. Liquids with permanent porosity. *Nature* 2015;527:216-20. DOI

38. Rimsza JM, Nenoff TM. Porous liquids: computational design for targeted gas adsorption. *ACS Appl Mater Interfaces* 2022;14:18005-15. DOI PubMed

39. Kim T, Park JY, Hwang J, Seo G, Kim Y. Supramolecular two-dimensional systems and their biological applications. *Adv Mater* 2020;32:e2002405. DOI

40. Shi L, Lu S. Precise carbon dots synthesis: building bridges between organic chemistry and inorganic chemistry. *Sci Bull* 2022;67:2369-71. DOI PubMed

41. Shi L, Wang B, Lu S. Efficient bottom-up synthesis of graphene quantum dots at an atomically precise level. *Matter* 2023;6:728-60. DOI

42.   Han X, Guo C, Xu C, et al. Water-soluble metallo-supramolecular nanoreactors for mediating visible-light-promoted cross-dehydrogenative coupling reactions. *ACS Nano* 2023;17:3723-36. DOI

43.   Zheng S, Xu Y, Su P, et al. Anion-induced differential assembly and structural transformation of supramolecular coordination cages. *Chinese Chem Lett* 2023:108477. DOI

44.   Liu W, Liu G, Zhu X, et al. Tailored metal-organic tetrahedral nanocages with aggregation-induced emission for an anti-counterfeiting ink and stimulus-responsive luminescence. *New J Chem* 2022;46:8062-8. DOI

45.   Miao L, Zhu X, Liu G, et al. Tunable aggregation-induced fluorescent and pressure-responsive luminescence supramolecular cages achieved by subcomponent self-assembly. *Chinese Chem Lett* 2023;34:107921. DOI

46.   Wang QQ, Day VW, Bowman-James K. Chemistry and structure of a host-guest relationship: the power of NMR and X-ray diffraction in tandem. *J Am Chem Soc* 2013;135:392-9. DOI PubMed

47.   Zhang D, Ronson TK, Greenfield JL, et al. Enantiopure $[Cs^+/Xe \subset Cryptophane] \subset Fe^{II}_4L_4$ hierarchical superstructures. *J Am Chem Soc* 2019;141:8339-45. DOI

48.   Liu X, Shi Z, Xie M, et al. Single-handed double helix and spiral platelet formed by racemate of dissymmetric cages. *Angew Chem Int Ed Engl* 2021;60:15080-6. DOI

49.   Fantozzi N, Pétuya R, Insuasty A, et al. Selective detection of choline in pseudophysiological medium with a fluorescent cage receptor. *Org Lett* 2023;25:2444-9. DOI

50.   Chakraborty S, Newkome GR. Terpyridine-based metallosupramolecular constructs: tailored monomers to precise 2D-motifs and 3D-metallocages. *Chem Soc Rev* 2018;47:3991-4016. DOI PubMed

51.   Chen Y, Wu G, Chen B, et al. Self-assembly of a purely covalent cage with homochirality by imine formation in water. *Angew Chem Int Ed Engl* 2021;60:18815-20. DOI

52.   Harris K, Fujita D, Fujita M. Giant hollow M_nL_{2n} spherical complexes: structure, functionalisation and applications. *Chem Commun* 2013;49:6703-12. DOI

53.   Yan LL, Yao LY, Ng M, Yam VW. Stimuli-responsive and structure-adaptive three-dimensional gold(I) cluster cages constructed via "de-aurophilic" interaction strategy. *J Am Chem Soc* 2021;143:19008-17. DOI PubMed

54.   Ono K, Iwasawa N. Dynamic behavior of covalent organic cages. *Chemistry* 2018;24:17856-68. DOI PubMed

55.   Wilson A, Gasparini G, Matile S. Functional systems with orthogonal dynamic covalent bonds. *Chem Soc Rev* 2014;43:1948-62. DOI PubMed

56.   Frank M, Johnstone MD, Clever GH. Interpenetrated cage structures. *Chemistry* 2016;22:14104-25. DOI PubMed

57.   Montà-González G, Sancenón F, Martínez-Máñez R, Martí-Centelles V. Purely covalent molecular cages and containers for guest encapsulation. *Chem Rev* 2022;122:13636-708. DOI PubMed PMC

58.   Wang H, Jin Y, Sun N, Zhang W, Jiang J. Post-synthetic modification of porous organic cages. *Chem Soc Rev* 2021;50:8874-86. DOI

59.   Quan MLC, Cram DJ. Constrictive binding of large guests by a hemicarcerand containing four portals. *J Am Chem Soc* 1991;113:2754-5. DOI

60.   Bravin C, Badetti E, Licini G, Zonta C. Tris(2-pyridylmethyl)amines as emerging scaffold in supramolecular chemistry. *Coordin Chem Rev* 2021;427:213558. DOI

61.   Fernández-Caro H, Lostalé-Seijo I, Martínez-Calvo M, Mosquera J, Mascareñas JL, Montenegro J. Supramolecular caging for cytosolic delivery of anionic probes. *Chem Sci* 2019;10:8930-8. DOI PubMed PMC

62.   Hashikawa Y, Murata Y. Probing the regioselectivity with encapsulated H_2: diels-alder reaction of an open-cage C_{60} derivative with anthracene. *Chemistry* 2019;25:2482-5. DOI

63.   Plessius R, Orth N, Ivanović-Burmazović I, Siegler MA, Reek JNH, van der Vlugt JI. Reversible multi-electron storage in dual-site redox-active supramolecular cages. *Chem Commun* 2019;55:12619-22. DOI PubMed

64.   Wu SY, Guo XQ, Zhou LP, Sun QF. Fine-tuned visible and near-infrared luminescence on self-assembled lanthanide-organic tetrahedral cages with triazole-based chelates. *Inorg Chem* 2019;58:7091-8. DOI PubMed

65.   Bhatta SR, Mondal B, Vijaykumar G, Thakur A. ICT-isomerization-induced turn-on fluorescence probe with a large emission shift for mercury ion: application in combinational molecular logic. *Inorg Chem* 2017;56:11577-90. DOI PubMed

66.   Yan Z, Lei H, Li N, Hong L. Preparation of 4,4'-bis-(carboxyl phenylazo)-dibenzo-18-crown-6 dye and its application on ratiometric colorimetric recognition to Hg^{2+}. *Spectrochim Acta A Mol Biomol Spectrosc* 2011;79:661-5. DOI PubMed